HHS Public Access

Author manuscript

Acta Biomater. Author manuscript; available in PMC 2022 April 15.

Published in final edited form as:

Acta Biomater. 2021 April 15; 125: 172–182. doi:10.1016/j.actbio.2021.02.028.

Effects of Recipient Age, Heparin Release and Allogeneic Bone Marrow-derived Stromal Cells on Vascular Graft Remodeling

Richard Johnson[1], **Michael Rafuse**[1], **Prakash Parthiban Selvakumar**[1], **Wei Tan**[1]

[1]Department of Mechanical Engineering, University of Colorado at Boulder, Boulder, CO

Abstract

Small-caliber vascular grafts are used in a wide range of clinical conditions. However, there remains a substantial unfulfilled need for readily-available, synthetic vascular grafts with high long-term patency rate. To fulfill the translational goal for bioengineered vascular grafts, important considerations for the pre-clinical evaluation include the graft design, cell incorporation and selection of an animal model. To assess the three factors, we used vascular grafts consisting of core/shell-structured microfibers of polycaprolactone/gelatin with a thin polycaprolactone overlay. The respective influences of the heparin release mode, animal age, and allogeneic bone marrow-derived stromal cells (MSCs) seeded in the lumen on the graft remodeling were assessed after four-and-half-month implantation on an interposition graft of abdominal aorta model. Except two rats dying from graft-unrelated issues, all other rats (18 out of 20) showed good graft patency upon explantation. The cell phenotype, matrix content and structure in the neotissues around the graft, as well as the flow perfusion through the graft were examined. More grafts in the aged rats showed local narrowing and flow incongruence than the other grafts in young adult rats. Compared to acellular grafts, cellular grafts showed efficient recruitment of vascular cells to form more organized structures with elastin in the vascular wall. Endothelialization and α–smooth muscle actin-positive cells were shown in all four types of vascular grafts. This study revealed the significant effects of MSC and recipient age but not heparin release pattern on graft remodeling.

Graphical Abstract

Declaration of interests

The authors declare that they have no known competing financial interests or personal relationships that could have appeared to influence the work reported in this paper.

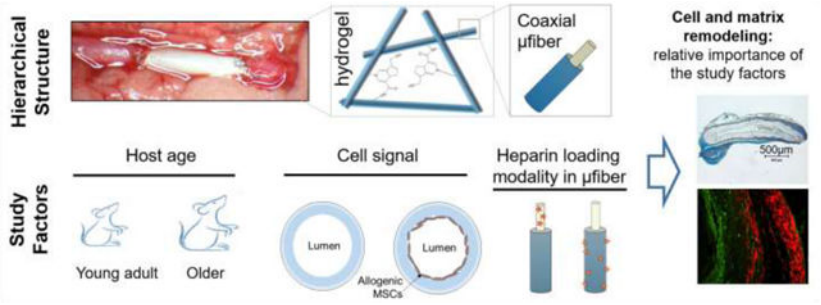

1. INTRODUCTION:

Vascular grafts play a critical role in the contemporary management of a wide range of clinical conditions, including coronary arterial diseases, peripheral arterial diseases, aortic aneurysm and congenital malformation.[1] While large-sized grafts possess great success rate, small- or medium- sized diameter (< 6mm) grafts do not. The first choice for these grafts is always an autologous blood vessel such as saphenous vein, due to its higher patency rate compared to synthetic grafts. However, prior surgeries and comorbid medical conditions such as diabetes mellitus limit the availability of a patient's own vessels. Also, vessel harvesting can cause complications, and may not be a solution for urgent medical situations. Therefore, in numerous circumstances, synthetic materials associated with high rates of thrombus formation and intimal hyperplasia must be used. [1,2] There remains a substantial unfulfilled need for readily available, small-caliber synthetic vascular grafts with high long-term patency rate.

To achieve the ultimate clinical translation of vascular grafts, recent studies have shifted the graft development from *in vitro* engineered tissue cultures to *in situ* regeneration, which focus on functional aspects of graft remodeling *in vivo* and logistical considerations about graft fabrication.[3,4] From a functional standpoint, an ideal graft provides properties and cues to guide vascular regeneration *in situ,* permitting vascular cell ingrowth and matrix production.[5] It is well accepted that tissues with mimetic arterial content could provide better graft performances than synthetic materials, due to reduced long-term complications such as thrombosis, intimal hyperplasia and aneurysmal dilation.[6] Logistically, the graft manufacturing process should be of short production time and result in products that are easy to store and use, in order to optimize 'off-the-shelf' capability.

To fulfill these goals set for graft function and fabrication, new approaches to graft materials and cell protocols have been respectively developed to incorporate proper micro-environmental cues that guide *in situ* graft remodeling.[1,7,8] Biochemicals ranging from small molecules to growth factor proteins are often used as instructive cues on grafts. Heparin (~7 kDa), the most often-used molecule for graft coatings, is a highly-charged polysaccharide playing an important role in lowering thrombogenicity by decreasing the platelet adhesion and facilitating vascular regeneration through its function as endothelial attractant.[9,10] Heparin may be attached permanently to the graft surface or more often temporarily released from the graft.[11,12] Though the availability of heparin molecules is essential for preventing thrombosis after the implantation, the impact of heparin loss, due to

its release into the surrounding tissue and blood, on the graft remodeling over the time is unknown. Cells, particularly stem cells, can also be strategically incorporated into grafts to assist graft remodeling. Adult stem cells such as bone marrow stromal cells (MSCs) are often considered for cell therapy in clinic. MSCs possess genetic integrity, low immunogenicity, anti-thrombogenicity, and immunomodulatory properties.[8,13,14] They also present multi-potent capacity by differentiating into vascular cells or secreting functional molecules that benefit healing or regeneration. However, a logistic consideration for translating the MSC use to the clinic is the time involved in the cell culture and differentiation. In this study, we incorporated heparin into grafts with different release modes and seeded allogeneic MSCs onto the graft lumen with minimal culture time, in order to investigate their relative significance to the long-term graft remodeling *in situ*.

Another important consideration during the pre-clinical evaluation of vascular grafts is the selection of an animal model. While recent studies have evaluated graft performances in different animal species,[15,16] the importance of animal age remain relatively under-explored. It is increasingly realized that the choices of the developmental stage of animals play a pivotal role in determining tissue remodeling or regeneration.[17] The performances of vascular grafts are often assessed with juvenile animals with high regenerative potential and few health complications. The success in clinical trials of vascular grafts is more noticeable in children than adult patients. [18,19] As cardiovascular diseases increase exponentially with age, a properly aged model would be important to reflect clinical patho-physiological conditions for the sake of graft patency and performance assessment.[16,20] The life stage of an animal model significantly affects repair ability and cell metabolic activities. [21,22] Due to a decreased metabolic rate and/or abnormal metabolism, aged animals may better simulate many clinical situations.

The present study involves the use of our developed graft materials while employing three factors, heparin incorporation into the graft (heparin release mode), seeded MSC and animal age, to evaluate their respective influences on graft remodeling after four and half month implantation. The graft remodeling, in terms of the changes in cells, matrices and graft structures, as well as the flow perfusion through graft implants, were examined in this preclinical assessment. These outcome measures provided important information regarding the study design for graft evaluations.

2. MATERIALS AND METHODS:

Unless specified otherwise, all polymers and chemicals, including poly-ε-caprolactone or PCL (Mn = 80,000), gelatin, 2,2,2 trifluroethanol, methanol, and 1,1,1,3,3,3 hexafluoro-2-propanaol (HFP), were purchased from Sigma Aldrich Inc. (St Louis, MO).

2.1. Material fabrication

The apparatus used for obtaining coaxial fibers was developed in house. The core hydrophobic polymer solution was passed through the inner needle of 22 G (internal diameter of 0.71 mm) and the shell gelatin solution was passed through the outer needle of 16 G (internal diameter of 1.65 mm). A dual syringe holder was used to place the syringes loaded with polymer solutions. This design allows the solutions to be extruded

simultaneously. Following our established protocol,[23] polymer solutions with 1% (w/v) concentration of PCL, and 5% (w/v) of gelatin were prepared by dissolving the predetermined amount of PCL or gelatin in HFP. HFP is a miscible solvent system with strong acidity and good electrical conductivity, which assists the blending of hybrid (synthetic/natural) polymers of PCL/gelatin for electrospinning by reducing the surface tension in polymer solutions and enabling the use of low polymer concentrations. The solutions obtained after stirring for 6 to 8 hours were loaded in 5 mL syringes connected to the positive terminal of a high voltage ES30P 10 W power supply (Gamma High Voltage Research, Ormond Beach, FL). The polymer solutions were extruded at 1 mL/h using syringe pumps (Pump 11 Plus, Harvard Apparatus, Boston, MA) and was subjected to an electric potential of 1kV/cm. The fibers were deposited onto a cylindrical aluminum rod of 1.25mm in diameter rotating at 150rpm and placed at a distance of 11 cm perpendicular to the needle. To facilitate detachment of scaffold materials from the collector and protect the scaffold lumen surface, the collector was tightly wrapped with a thin aluminum foil with an ultrathin PEO layer covering its surface. PEO fibers electrospun prior to PCL were dissolved in DI water, and released PCL/gelatin fibers from the foil. The aluminum rod was coupled to a BMU230AP-A-3 brushless DC motor (Oriental Motor Corp, USA). Because our previous study showed that the nanofibrous material made of PCL-gelatin of 1:5 (weight ratio) was compliant (i.e. an average compliance of 30%) but not strong enough as grafts (i.e., an average burst strength of 380mmHg),[23] a thin capping layer of PCL was utilized around the PCL-gelatin coaxial fibers. The PCL-gelatin coaxial fibrous layer was spun for 35 minutes up to a thickness of 120μm, which was followed by spinning 6% (w/v) of PCL for 10 minutes with a thickness of approximately 30 μm. The solution of 2,2,2 trifluroethanol was used as the solvent to electrospin the capping polymers with the same electrospinning parameters as those for the coaxial electrospinning. The obtained samples were stored at the room temperature until further use. The theoretical degradation period of the scaffold is two to three years for PCL and shorter than a month for crosslinked gelatin.

Genipin (Wako Chemicals, Japan) was used to crosslink electrospun fibers. The scaffolds composed of coaxially electrospun fibers were subjected to crosslinking for 24 hr by immersion in the solution containing 0.25 % (w/v) genipin dissolved in 100% ethanol and then 24 hr in the solution containing 0.25 % (w/v) genipin dissolved in water. Immediately after the crosslinking process, fibrous scaffolds were rinsed with phosphate buffered saline (pH 7.4). Prior to implantation, the cleaning and sterilization of grafts were performed by immersing them in 70% ethanol for 0.5hr before transferring to 1x concentration of Pen/Strep (CellGro products from Corning Life Science, Corning, NY) in PBS for 24 hr. The grafts were also lyophilized for 48 h for imaging under scanning electron microscopy (SEM).

This study involved four graft groups: (i) heparin-immersed (HI) group, (ii) heparin-impregnated (HIP) group, (iii) HIP with MSCs seeded in the graft lumen (HIP + MSC), and (iv) HIP implanted in aged animals (HIP +Age). Heparin is a thrombo-resistant molecule and endothelial attractant. Samples for HI grafts were prepared by immersing the crosslinked graft in sterile 0.5% heparin solution in PBS for 24 hr at room temperature. Samples for HIP grafts were prepared by first dissolving heparin in sterile DI water.[24] Then, methanol was added slowly at 40μl increments to keep heparin from precipitating out,

obtaining a heparin-methanol solution (8% wt). PCL was dissolved in HFIP to obtain an 8% stock PCL solution, which was then added slowly to the heparin-methanol solution for a final ratio of 3:7 (methanol to HFIP). Successful mixing achieved a white opaque colloidal solution of heparin particles. The total heparin concentration in the resulting PCL solution was 0.5% by weight.

2.2. Electron microscopy imaging of fiber structure

The nanostructure of the coaxial fibers was observed using H7650 transmission electron microscope (TEM; Hitachi Ltd, Tokyo, Japan) operated at 80 kV. The electrospun nanofiber samples for TEM observation were prepared by directly depositing the as-spun fibers on carbon-coated TEM grids.

To examine fiber morphology in the graft materials, aluminum substrates coated with the electrospun fibers were mounted on brass stubs and sputter coated with Pt/Pd (Cressington Sputter Coater, Cressington Scientific Instruments, Watford, UK). Imaging was performed at 5 kV by using a field-emission SEM (Hitachi SU3500, Hitachi High Technologies America, Schaumburg, IL). Both uncrosslinked dry fibers and crosslinked electrospun fibers were analyzed.

2.3. Cell retrieval, culture and seeding

The MSCs were obtained from allogeneic rats with an age of 7 months. After animals were sacrificed, their femur was removed aseptically and placed in cold PBS. Bones were then dissected in the culture hood, and bone marrow was flushed out with culture media using 25 gauge needle into the medium stock in sterile tubes. Finally, clumps of marrow were dissociated and suspension were drawn for filtration and centrifugation. Collected MSCs were placed into fresh tube for cell seeding. MSCs were cultured in the DMEM media supplemented with 10% stem cell qualified FBS from Atlanta Biologicals (Flowery Branch, GA) and 1% penicillin-streptomycin from Thermo Fisher to proliferate until confluency. To confirm the stemness of rMSCs, were cultured to confluence in a 12-well plate. Cells were probed with immunofluorescent staining and/or qPCR, by showing the presence of CD44 and CD73 and the absence of CD31 and CD34 for removal of endothelial progenitor or hematopoietic cells. The rat arterial endothelial cells were used as a control for the phenotypic determination. MSCs with passages 3–6 were used in the *in vitro* cell characterizations and implantation. Prior to cell seeding, the graft, suture strings and adapters were sterilized in 70% ethanol for 1 hr. All jackets and plugs used in the seeding process were autoclaved for 20 minutes. The vascular grafts were then rehydrated by soaking in sterile DPBS and then medium with FBS. The centrifuge method was used to seed MSCs onto the surface of the graft lumen, using modified protocols reported previously. This was started by securing one end of the graft with an adapter plug with sutures. Then, the suspension of freshly-detached cells with a density of 2×10^6 cells/mL was obtained. After filling the space in the graft lumen with the MSC suspension, the other end of the graft was secured with an adapter plug. Custom-made jacket rings were then wrapped around the graft to fit it into a centrifuge tube and adapter spacer rinds were placed around both adapters. The fully-assembled centrifuge tube was then placed in the center of a centrifuge. The tube was aligned perfectly to the center to avoid any wobbling or uneven

spinning. Then, the system was allowed to spin at 2000 rpm for 5 minutes with centrifuge seeding. Finally, the graft secured with the adapters was allowed to sit for about an hour before carefully removing the adapters. Post-seeding culture time time is about one day before implantation.

2.4. Heparin Release Assay

Around 1 cm section of heparin impregnated graft were submerged in 1 ml of PBS and incubated at 37°C. At the time points of 1, 3, 5, 7, 14, 21 and 28 days, the 1ml volume of PBS was extracted for heparin content measure and replaced with fresh DPBS. The Biophen heparin Anti-Xa Assay/Detection Kit (HYPHEN BioMed, Mason, OH) was used to detect the amount of heparin released during each time point. Heparin Anti-Xa method is a two-stage chromogenic assay capable of measuring for their Anti-Xa activity of homogeneous heparin in plasma or in purified solutions.

2.5. Vascular Graft Implantation

The animal experiments were approved and performed according to the Institutional Animal Care and Use Committee (IACUC, approval number: 1407.02) at the University of Colorado and complied with the NIH's Guidelines for the Care and Use of Laboratory Animals. The implantation of vascular grafts was performed on a total of twenty Sprague Dawley rats (ENVIGO, Indianapolis, IN), but one with HI graft died prematurely after 14 weeks and one with MSC-seeded HIP graft died soon after the surgery appearing to be caused by surgical infection. Thus, a total of eighteen rats were used in the study, which included fourteen at 8–9 months old and four at 17–18 months old at the time of the implantation, weighing 398 ± 5 grams (n = 14) and 465 ± 12 grams (n = 4), respectively. There is a statistically significant difference ($P<0.001$) in body weight between aged and young groups (Figure S1).

For the four study group (HI, HIP, HIP+MSC, HIP+Age), each group had 4–5 rats that were successfully explanted. At the time of explantation, no aneurysmal changes were observed in any graft implants. The patency rate was 100% for each study group, though. For the two rats that died during the course of implant evaluation, we noted no blood in abdominal cavity and grafts intact with no blood clotting or narrowing in the graft. Anesthesia in rats was induced with 5% isoflurane gas (Vet One) and maintained with 2% isoflurane gas. Surgical site was cleaned and disinfected with povidone-iodine (Medline Industries Inc, Northfield, IL). Abdominal incision was made down the midline into the abdominal cavity to access abdominal aorta. The abdominal aorta was dissected away from the inferior vena cava and camped off upstream and downstream of the implantation site. A small section (~1cm) of aorta was removed to where the graft with a 1.5 mm diameter was anastomosed in an end-to-end fashion using twelve continuous surgical stitches at each anastomosis sit of the graft. After completion of the anastomosis, the clamps were removed to restore arterial perfusion and the anastomosis inspected for leakage. The incision was then closed in a routine fashion using running stitches with 5G vicryl sutures for the abdominal muscle layer and 9m (Kent Scientific) wound clips for outer hide closer. The animals received 50/50 mix of lidocaine 1–2% with 0.5% bupivacaine on incision line using a 1 ml syringe as well as 4 mg/kg body weight dose of meloxicam (0.3mg/kg) after the surgery. Follow-up examinations were performed twice a day in the first three days and then weekly after that.

During these examinations, no rats were found to experience any obvious discomfort, edema, swelling, weakened thrill or other neurologic disorders. No complications such as hemorrhage were revealed upon explantation.

2.6. Ultrasonograph, Doppler and Graft Explantation

Prior to graft explantation, the vascular graft morphology as well as blood flow pattern and flow velocity through the grafts were obtained with ultrasonographs and doppler colorimetric measurements. Briefly, rats were anesthetized with isoflurane gas after four and a half months of implantation and shaved around the area of implant with ultrasound gel applied thereafter. Ultrasound imaging and measurements were taken with ACUSON SEQUOIA™ 512 ultrasound system (Siemens Medical Solutions, Mountain View, CA) after graft sections were located using color doppler methods. The linear array ultrasound transducer was used to probe graft morphology and flow in both transverse section and cross section from the vertical aspect. After imaging, rats were immediately euthanized via CO_2 asphyxiation and samples including the upstream artery, downstream artery, graft and graft-artery anastomosis, were taken. Portions of all samples were saved in All-protect (Qiagen, Hilden, Germany) and 10% Formalin for PCR and histological analyses, respectively.

2.7. Histochemistry, Immunofluorescence and immunohistochemistry

Samples of the graft, upstream vessel, downstream vessel and neighboring arteries were fixed and stored in 10% formalin (or 3.7% formaldehyde). Samples for immunofluorescence were embedded in cryostat embedding medium (Tissue Tek, Torrence, CA) and sectioned with a cryostat at −20°C. Samples for histology or histochemistry were embedded in paraffin blocks.

Histological sections were stained with trichrome stain, and observed under a light microscope at varied magnifications. Sections with 5–10 micron thickness were cut through the transverse plane and collected onto glass slides. Samples slides were stained using the protocol outlined from the trichrome staining kit (Mastertech, McKinney, TX), and imaged using a Zeiss Axioskop 40. Trichrome staining provided a rough histological evaluation, including the cell density and extracellular matrix content. Histological analysis of fibrillar collagens was evaluated with stain and imaged under a polarized, brightfield microscope performed to better understand matrix remodeling around vascular grafts. To confirm the collagen content resulted from multiphoton imaging, picro sirius red stain was used here. This stain could enhance the natural birefringence of collagen fibers while imaged with polarized light. Briefly, the collagen content was visualized by staining tissue sections with 0.1% (m/v) picro sirius red F3B (Vector Laboratories, Inc., Burlingame, CA) in saturated aqueous picric acid for 1 hr, and then rinsing in two changes of acidified water (0.5% acetic acid) for 2 min each. The stained samples were then dehydrated using graded ethanols, cleared, and mounted on slides with synthetic resin. Cross-polarized bright field microscopy was used to capture images from representative areas of samples, using a 40x objective lens and a mounted digital camera system.

Immunohistochemistry was performed according to the avidin biotinylated-HRP complex (ABC, Vector Laboratories) method using an ImmunoCruz ABC kit (Santa Cruz

Biotechnology Inc, Dallas, TX) by following the manufacturer's protocol. Glass slide mounted paraffin imbedded sections were cleared and rehydrated using histoclear then transferring the tissue through solutions of increasing water to alcohol concentration, until 50% water to alcohol is reached followed by 5 minute rinse in water. Antigen retrieval was done for 5 min in a cooker using sodium citrate buffer (10mM). Slides were washed twice with 0.1 M tris base-buffered saline (TBS, Santa Cruz Biotechnology, Dallas, TX), pH 7.4 and pretreated for 30 min with 3% hydrogen peroxide in 0.1 M TBS to quench endogenous peroxidase. Serial sections were then incubated for 30 min at the room temperature in a blocking solution containing 3% serum in TBS for 3 hours and probed overnight with primary antibody directed against αSMA (Abcam, Cambridge, MA), appropriately diluted in TBS containing 0.05% Triton X-100 and 0.5% serum. On the following day, sections were rinsed in TBS (2 × 10 min) and incubated for 45 min at room temperature in biotinylated IgGk binding protein in TBS, followed by 45 min in ABC solution (prepared according to the manufacturer's instructions). Visualization of bound peroxidase was achieved by reaction for 10 min in premixed ImmPACT NovaRED peroxidase substrate and Gills formula hematoxilyn counterstained following product instructions. Slides were then dehydrated with increasing concentrations of EtOH and cleared with histoclear prior to mounting with coverslips and imaged using a light microscope (Nikon).

Immunofluorescent staining of vWF and CD68 was obtained using anti-Von Willebrand Factor antibody conjugated to FITC (Abcam, Cambridge, MA) and anti-CD68 (Santa Cruz Biotechnology), respectively. Slides were rehydrated and antigen retrieval processed following the same method as with immunohistochemistry staining above. Slides were blocked in appropriate concentration goat serum and probed overnight at 4°C at a dilution of 1:100. Coverslips applied with vectasheild mounting medium with DAPI for counter-stain (Vector Laboratories, Burlingame, CA) and imaged with a florescent microscope (Nikon, Instruments Inc., Melville, NY).

2.8. Dual-modality Multiphonton Imaging with Secondary Harmonic Generation and Fluorescence Excitation

Dual multiphoton imaging modality, including second harmonic generation (SHG) and two-photon excitation fluorescence (TPEF), was used to respectively investigate the fibrillary collagen and elastin contents. Samples were dehydrated, sectioned and mounted on glass slides. For SGH and TPEF imaging of collagen and elastin, slides were deparaffinized with histoclear, hydrated, and submerged in PBS. The sections were then covered with a coverslip, and imaged using a confocal laser scanning microscope system (Radiance 2000 MP, Bio-Rad Laboratories Inc, Hercules, CA) with 40x magnification (n.a. = 1.30), oil immersion objective. A femtosecond pulsed laser system tuned to 860nm wavelength was used for excitation (Spectra-Physics, MaiTai wideband, mode-locked Ti:Sapphire laser system). The response signal was split at 455nm using a dichroic mirror (AT455 DC, Chroma Technology Corp, Bellows Falls, VT). Collagen SHG signal (400–455nm) and elastin TPEF (460–610nm) signals were captured simultaneously using the direct detector system (Bio-Rad). A 535/150 nm BrightLine bandpass filter was used for elastin TPEF capture. Images 1024×1024 pixels (305×305 microns) were collected at 50 lps. Each image was generated using Kalman averaging over 3 frames.

2.9. Gene Expression Analysis

Tissue mRNA collection and purification were completed using Direct-zol RNA Miniprep Plus kit (ZYMO Research Corp, Irvine, CA). Tissue lysis was performed on graft samples at a sample to Trizol ratio less than 10% (graft tissue / buffer). The lysis were done by a hand homogenizer (Cole Parmer) on ice for 20 sec bursts for 1 min total on ice in TRI reagent from the Miniprep Plus kit. The mRNA purification was performed following the instructions from ZYMO kit. The concentration of purified mRNA, with a final volume of 50 μl in dnase/rnase-free distilled water, was measured with NanoDrop 2000 (Thermofisher). The cDNA synthesis was performed using iScript reaction mix (BioRad) with a 20μl reaction volume. In a 200μl vial, 4μl 5x iScript Reaction Mix, 1μl iScript Reverse Transcriptase and mRNA samples were combined Thermal cycle was completed at reaction times and temperatures as advised by BioRad iScript protocol instructions to complete cDNA synthesis. qPCR analysis was performed using iTaq universal SYBR Green Supermix (Bio Rad). The sample cDNA (5μg) was combined with 10ul iTaq universal SYBR Green supermix plus Forward and reverser primers (Real Time Primers LLC, Elkins Park, PA). Thermal cycling protocol was performed as follows; 5 minutes denaturing step at 95°C, 20 sec annealing/extension and plate read at 60°C for 45 cycles followed by Melt curve analysis from 65°C to 95°C (0.5°C increments) at 3 sec/step. Data calculations were done following the Livak method of ΔΔCq analysis.

2.10. Data analysis and statistics

Unless otherwise specified, all the data presented were the mean values quantified from at least three independent experiments. Error bars on all the graphs represented the standard deviation of the mean based on the total number of the samples. Prizm software was used for performing statistics and plotting graph. Data were statistically analyzed using the one-way analysis of variance test. Student's t test was then used to compare the means of each individual group. The level of statistical significance was set at a $\alpha = 0.05$ for 95% confidence. For each experiment for microscopy images, at least four sampling regions were analyzed.

3. RESULTS:

All rats except two successfully went through graft implantation procedures and survived, until they were sacrificed for explantation. The deaths of two deceased rats were likely due to surgical or animal-related issues with no noticeable adverse events related to the grafts. Overall, the good patency, graft integration and restoration of pulsatile flow through the grafts were noted in all cases. Explants revealed little complications in rats. Upon explantation, grafts were well connected with the native arteries at anastamosa. To evaluate the respective impact of the heparin release pattern, MSC seeding and animal age, the grafts were analyzed in terms of flow through the graft, tissue formation, as well as matrix and cell remodeling.

3.1. Characterizations of graft materials

Figure 1 shows the design, characterization and implantation of vascular grafts. The design of vascular grafts is characterized by microfibers coaxially structured with a PCL core and a

gelatin shell (Figure 1A-B); the shell can be hydrated and crosslinked into a hydrogel network. Representative SEM images of a crosslinked coaxial fiber scaffold and an uncrosslinked fiber scaffold were shown in Figure 1C and Figure S2A, respectively. The average fiber diameter (207 ± 39 nm) and average pore size in the crosslinked samples were both significantly larger than those in the crosslinked samples, while the porosity was reduced in the crosslinked samples (Figure S2B-D). This was likely caused by the swelling of gelatin shell during the crosslinking process.

To demonstrate the difference in heparin release between HI and HIP grafts, the temporal release profiles were determined (Figure 1D). The results showed that HI and HIP grafts released a total of 91 ± 4% and 22 ± 6% heparin, respectively, within the first 24 hours; after 3 days, these dropped to 97 ± 2 % and 52 ± 2 %, respectively; and after 21 days, 99 ± 1 % and 95 ± 5 %, respectively. Therefore, the HI grafts released the majority of heparin in the first 24 hours, while the HIP grafts showed much steadier release profiles in the first 3 weeks.

For the HIP+MSC group, allogeneic MSCs were seeded in the graft lumen to form a uniform cell sheet and used within one day (Figure 1E). Four types of grafts were similarly implanted (Video S3). The graft size matched well with neighboring arteries (Figure 1F). Upon explantation, the vascular grafts remained separated from neighboring tissues and consistently well integrated with native arteries. No obvious tissue encapsulation was found in any case.

3.2. Ultrasonography imaging of flow and graft

The doppler videos (Videos S4 A-D) and images (Figure 2) as well as ultrasonography images (Figure S5) were used to detect the flow profile and graft diameter *in vivo*. The doppler images taken just before explantation revealed that all four types of vascular grafts remained patent with no obvious occlusion or dilatation at any graft cross-section, neighboring arteries, or graft-artery anastamosa. Local narrowing of graft lumen at the anastomosis or graft was noted for 75% of the grafts implanted in aged rats (HIP + age), resulting in flow incongruence. Narrowing to a more limited extent (10–20%) was found in fewer (20–25%) grafts for all the other three graft types implanted in younger adult rats, which did not cause obvious flow incongruence, suggesting satisfactory graft-artery integration. Additionally, the mean value of peak flow velocity and pulsatility in the grafts implanted in aged rats were much lower than those implanted in younger adult rats (Figure S5A), further underscoring the role of age in the grafting outcome. Furthermore, the tissue B-mode ultrasonography images were used to estimate changes in the graft diameter (Figure S5B). Analysis of these images revealed no significant changes in the mean lumen diameters for all graft types (Figure S5C), which were close to the corresponding size of neighboring arteries. Figure S5D illustrates why the flow velocity was reduced in stenosed grafts in aged rats. Stenosis at the two anastomosis sites caused flow disturbance restricting the flow across the graft, thus reducing the flow velocity in the mid-graft section, where the flow velocity was measured.

3.3. New tissue formation around vascular grafts

To assess the gross remodeling of the grafts, Figure 3 shows the grafts with trichrome stain on histological sections. In these images, the cells appeared in pink, muscle in red, and collagen fibers in blue. The histochemical analyses revealed the neotissue formation in both luminal and abluminal areas, leading to overall thickening for all grafts. Among all grafts, the neotissues were most prominent around the cellular grafts, where the cell infiltration and matrix production were significantly more than the other types of grafts. Neotissues grew in both luminal and abluminal spaces of other grafts, with nearly matched thickness except cellular grafts. Compared to other grafts, neotissues around grafts in aged rats seemed less dense in the collagen content, while some intimal hyperplasia appeared to locally narrow the lumen. This was consistent with the ultrasonic graft morphology images and Doppler flow imaging. Delamination of the grafts at some locations was found in all grafts. This likely resulted from graft tissue sectioning. Due to the slow degradation rate of PCL, we expect that the majority of grafts remained undegraded after 4.5 months *in vivo*. The overall thickness of new tissues around the grafts were approximately similar to that of a native abdominal aorta, except the cellular graft (Figure 3B), while the wall thickness of adjacent arteries remained constant in all cases (Figure S6).

3.4. Extracellular matrix (ECM) production around vascular grafts

In order to regenerate tissue mechanical properties, the production of structural matrix proteins is critical. The strength and elasticity of a native artery are contributed by its matrix components, mainly fibrillar collagens (predominantly types I and III) and elastin fibers.[25] Herein, we analyzed fibrillar collagens and elastin fibers in tissue sections (Figure 4), which were simultaneously and respectively imaged using multiphoton imaging modalities, TPEF and SHG. Results showed the collagen formation occurred in the neotissues around all four types of grafts, but few elastin fibers were produced around these grafts except the cellular grafts. Cellular grafts stimulated the production of elastin, significantly higher than the other three types of grafts. Furthermore, the circumferential alignment of the fibrillary collagen as well as the density and organization of elastin fibers in the cellular grafts appeared closer to those in the native artery than other graft types. However, the collagen fibers in the cellular graft appeared larger while the elastin fibers appeared smaller, fragmented or discontinuous, compared to a native artery. The other three types of grafts did not show noticable elastin signals. The animal age (HIP vs HIP + age) or heparin release profile (HI vs HIP) did not significantly affect collagen or elastin fiber formation. The collagen fibers in grafts from aged animals, however, appeared disoriented and less dense than those from younger adult animals. Heparin release profile seems to have minimal effects on the matrix production or tissue remodeling. To validate multiphoton imaging results, picrosirius red staining combined with polarized imaging was performed (Figure 4, Bottom panel), which revealed fibrillar collagen content that was consistent with SHG signals. Multiphoton imaging yielded accurate information about fibrillar collagen and elastin contents on unstained samples, with added benefits of high resolution and specificity for quantification and microstructural analyses to reveal the molecular order and fiber organization.[25]

3.5. Cell infiltration and remodeling around vascular grafts

Figure 5 shows the graft sections immuno-stained with antibodies against smooth muscle α-actin (α-SMA, vascular smooth muscle marker) and vWF (vascular endothelial marker), with DAPI as the counter stain for nuclei. Endothelialization (Figure 5, top panel, green label) were shown in all four types of vascular grafts. The immunofluorescent imaging of vWF revealed that the formation of continuous endothelial lining along the lumen of all the grafts from younger animals. Results with immunohistochemical staining of α-SMA$^+$ cells showed these cells appeared to be more abundant in the abluminal tissue closer to the lumen than the area in the outer region. The cellular grafts showed a number of elongated α-SMA$^+$ cells, which was in good agreement with matrix production results. Interestingly, the grafts from aged animals also displayed many α-SMA positive cells, but they appeared less elongated in shape, which might be migratory myofibroblasts. Figure S7 illustrated cells positive with CD68 (macrophage M1 phase marker), showing no presence of chronic inflammation in the grafts.

3.6. Gene expression

To confirm our findings in the matrix protein production and cell remodeling, genes (mRNA) were extracted and quantitative PCR analysis were performed on the cell phenotype markers as well as the ECM protein elastin. Figure 6 shows that the gene expression results generally agreed with the findings above, showing increased expression of α-SMA expression and elastin in the cellular grafts, which might be due to more abundant α-SMA positive, elastin-producing cells in the neotissues. Additionally, the gene results for the age group correspond to immunostaining and TPEF-SHG imaging results. As shown in immunostaining results (Figure 5), α-SMA appeared higher in the age group compared to the HI group, which might be α-SMA-positive myofibrotic cells contributing to lumen narrowing. The elastin gene expression in the age group was close to HI or HIP group but was much lower than HIP+MSC, which was consistent with the TPEF-SHG imaging of the ECM production in different types of grafts (Figure 4). Herein, vWF was used as a reference, due to its relatively stable expression among all grafts. A range of cell types appeared in grafts and the four types of grafts had very different cellular compositions, and thus widely-used control genes such as GAPDH or beta-actin, which were highly dependent on the cell type,[26–29] resulted as less suitable references. A limitation here lies in a smaller sample set available from All-protect for the age group excluding it from analysis of variance.

4. DISCUSSION

The present study using coaxial PCL-gelatin fiber grafts has revealed that the seeded MSC and animal age both significantly influenced vascular graft remodeling. We chose the PCL core as the structural component of our vascular graft, because its slow degradation rate maintained graft mechanics, while gelatin encouraged cellular integration. Co-axially structured PCL-gelatin provides a crosslinked soft hydrogel to interact with cells. Anti-thrombogenic heparin was introduced into the PCL core (HIP) and the gelatin (HI), respectively for varied release rates. This study is the first to investigate into the relative

influences of three factors, ranging from biomolecule in the graft, to cell and host factors, on the graft patency and tissue integration.

Various methods are being developed to engineer vascular constructs for small diameter vessels. Options include integrating small chemicals, growth factors, or cellular signals into the graft constructs. [30–32] Heparin is often bound to the graft lumen surface, due to its multiple roles in improving the graft patency. However, previous studies using heparin in the vascular graft application are limited in its role in reducing platelet adhesion and thus graft thrombosis, as well as promoting endothelial cell growth and thus graft endothelialization. Much less explored in the vascular graft application is the heparin effects on promoting a contractile SMC phenotype and preventing SMC proliferation. [11,33–35] Herein, via the heparin incorporation strategies in the nano-structured fibers, we examined the influences of heparin release pattern on altering SMC regeneration and graft performances *in vivo*. The prolonged heparin availability did not significantly change the SMC content and graft performance, which may be due to the slow degradation of PCL, which limited the SMC infiltration. This result is in agreement with previous study showing little impact of heparin on the ePTFE graft performances. [36] However, it is likely that heparin release pattern has a different effect on vascular tissue remodeling in the short term, [37] but the heparin effects reduce over the time. Nevertheless, as the long-term patency is the main topic for this study, we did not characterize any tissue remodeling at shorter time periods. Also, even if there were significant effects of heparin release on tissue remodeling in the short term, the effects in the long term were more decisive on the patency rates.

There is a dearth of literatures which consider the recipient age as an influencing factor for vascular grafting. However, if one is to consider the “real” clinical environment, it is the elderly who are typically the recipients of vascular grafting procedures and therefore, the age of the recipient is important.[22] This study showed that the age of recipient animals affected flow in the graft and tissue regeneration. Grafts in younger rats appeared to have less flow disturbance and healed with more organized ECM structures. Age is a significant determinant to the cell metabolism, proliferation and inflammation, as well as tendency to thrombosis.[21,38] The successful ECM formation requires the remodeling of graft materials by infiltrated host (or recipient) cells. To date, little attention has been paid into understanding grafting outcomes in adult recipients. Different from most vascular grafting studies, which used juvenile animals, we used animals with relatively older age; even the group with younger age was adult retired breeder rats. Optimal vascular grafting requires the integration, remodeling and functioning of the graft, which is highly dependent upon the recipient’s regenerative ability, primarily determined by the species, age and health condition. It is reasonable to expect that younger age represents recipients with high regeneration capacity.[22] Future studies can be designed to unravel combined effects of two study factors, for example aged recipients of grafts with seeded cells (i.e., rMSC + Age), which should have significant translational implications.

MSCs, autologous or allogeneic, have been used in vascular grafts. A major therapeutic impact of MSC *in vivo* may lie in their trophic, paracrine and immunomodulatory functions [39]. This study revealed cellular grafts resulted in thicker wall with more abundant ECM content after four-and-half-month of implantation, compared to acellular grafts. This could

be due to the trophic capacity of allogeneic MSCs, stimulating cells in the recipient rats to increase the tissue production for healing and regeneration. This result is in agreement with previous studies using allogeneic MSCs for anti-thrombogenesis and efficient recruitment of vascular cells to form more organized structures in the vascular wall.[40,41] However, when compared to cellular grafts in juvenile, immunodeficient rats in previous study, our cellular grafts showed more collagen production in young adult rats.[4] It is possible that the allogeneic cells, besides their pro-regenerative function, could induce acute immune response to enhance healing. Allogeneic MSC, categorized as a drug by regulatory agencies, was considered as a promising off-the-shelf therapy, because of their unique trophic signals for therapeutics. But a number of factors alter their therapeutic effects; the fate of implanted MSCs, particularly their secretion of bioactive signals, is tightly influenced by the microenvironment encountered. [39] The stimulus-responsiveness of the MSC can also explain the discrepancy in the MSC effect between this study and our previous study with a senescent sheep model, where ECM remodeling with collagen-rich, fibrotic-like tissues was more significant in acellular grafts than cellular ones. [42] The difference may be contributed by trophic signals of MSC in response to varied microenvironments at the graft site: (a) recipient animal difference in species and age (adult vs senescent); (b) donor MSCs from adult versus aged animals;[43] (c) graft surface for seeded cells – soft gelatin-sheathed coaxial fibers versus stiff PCL fibers in multilayered grafts; and (d) implantation site (abdominal aorta vs. carotid artery). All of these could greatly alter the cells' paracrine and immunosuppressive effects, thereby graft healing and tissue regeneration. Increasingly, however, *in vivo* studies reported that allogeneic MSCs, despite low immunogenicity, were not fully immune privileged, probably causing an immune response, which could further contribute to the differences we observed.[44]

Three limitations in the study must be acknowledged. First, we acknowledge the potential safety and regulatory concerns surrounding allogeneic cells, which make autologous cell therapies or acellular MSC products attractive alternatives for future regenerative studies. Recent studies demonstrate the efficacy of autologous MSCs,[32,45] and acellular MSC products such as extracellular vesicles in vascular grafts.[46] Second, the PCL core may not provide an optimal degradation rate for tissue integration. Rapid degradation of graft materials does not permit sufficient time for the production of adequate ECM components, resulting in aneurysm formation or graft rupture. Though slow degradation materials like PCL can provide mechanical support and prevent rupture of the grafts, they could cause long-lasting foreign body reaction within the grafts. Thus, there is a need to further study the effect of degradation rate on the matrix deposition and to develop grafts that are optimized to balance the degradation kinetics and ECM deposition. Third, we have not evaluated the survival and function of seeded cells. Nevertheless, we expect a significant loss of pre-seeded allogeneic cells from the implanted grafts under blood flow soon after implantation. [47–49] Though the effect of allogeneic cells may be transient due to cell loss, it is well accepted that the tropical effects of these cells through cytokines such as IGF [50] have significant impact on the grafts [51,52].

5. CONCLUSION

This study has evaluated the respective effects of the heparin release rate, allogeneic MSC and recipient age on the *in vivo* performances of the vascular graft. Using vascular grafts made of PCL/gelatin nano-structured coaxial fibers and an interposition graft of abdominal aorta model, we found all types of grafts remained patent without an indication of thrombosis after four-and-half-month implantation. We conclude that the seeded MSC and recipient age both significantly influenced graft remodeling and should be considered for future *in situ* grafting. In comparison, heparin release pattern from vascular grafts showed minimal influences on graft performances.

Supplementary Material

Refer to Web version on PubMed Central for supplementary material.

ACKNOWLEDGEMENTS

The research is partly funded by the NIH (NHLBI HL119371 to W. Tan).

REFERENCES:

[1]. Ong CS, Zhou X, Huang CY, Fukunishi T, Zhang H, Hibino N, Tissue engineered vascular grafts: current state of the field, Expert Rev. Med. Devices. 14 (2017) 383–392. 10.1080/17434440.2017.1324293. [PubMed: 28447487]

[2]. Dhulekar J, Simionescu A, Challenges in vascular tissue engineering for diabetic patients, Acta Biomater. 70 (2018) 25–34. 10.1016/j.actbio.2018.01.008. [PubMed: 29396167]

[3]. Wissing TB, Bonito V, Bouten CVC, Smits AIPM, Biomaterial-driven in situ cardiovascular tissue engineering—a multi-disciplinary perspective, Npj Regen. Med. 2 (2017) 18. 10.1038/s41536-017-0023-2. [PubMed: 29302354]

[4]. Pashneh-Tala S, MacNeil S, Claeyssens F, The Tissue-Engineered Vascular Graft—Past, Present, and Future, Tissue Eng. Part B Rev. 22 (2016) 68–100. 10.1089/ten.teb.2015.0100. [PubMed: 26447530]

[5]. Chang WG, Niklason LE, A short discourse on vascular tissue engineering, Npj Regen. Med. 2 (2017) 7. 10.1038/s41536-017-0011-6. [PubMed: 29057097]

[6]. von Bornstädt D, Wang H, Paulsen MJ, Goldstone AB, Eskandari A, Thakore A, Stapleton L, Steele AN, Truong VN, Jaatinen K, Hironaka C, Woo YJ, Rapid Self-Assembly of Bioengineered Cardiovascular Bypass Grafts From Scaffold-Stabilized, Tubular Bilevel Cell Sheets, Circulation. 138 (2018) 2130–2144. 10.1161/CIRCULATIONAHA.118.035231. [PubMed: 30474423]

[7]. Rocco KA, Maxfield MW, Best CA, Dean EW, Breuer CK, In vivo applications of electrospun tissue-engineered vascular grafts: a review, Tissue Eng. Part B Rev. 20 (2014) 628–640. 10.1089/ten.TEB.2014.0123. [PubMed: 24786567]

[8]. Gu W, Hong X, Potter C, Qu A, Xu Q, Mesenchymal stem cells and vascular regeneration, Microcirc. N. Y. N 1994. 24 (2017). 10.1111/micc.12324.

[9]. Gong W, Lei D, Li S, Huang P, Qi Q, Sun Y, Zhang Y, Wang Z, You Z, Ye X, Zhao Q, Hybrid small-diameter vascular grafts: Anti-expansion effect of electrospun poly ε-caprolactone on heparin-coated decellularized matrices, Biomaterials. 76 (2016) 359–370. 10.1016/j.biomaterials.2015.10.066. [PubMed: 26561933]

[10]. Olsha O, Goldin I, Shemesh D, Heparin-bonded expanded polytetrafluorethylene grafts in hemodialysis access, J. Vasc. Access. 17 Suppl 1 (2016) S79–84. 10.5301/jva.5000515. [PubMed: 26951912]

[11]. Yao Y, Wang J, Cui Y, Xu R, Wang Z, Zhang J, Wang K, Li Y, Zhao Q, Kong D, Effect of sustained heparin release from PCL/chitosan hybrid small-diameter vascular grafts on anti-

thrombogenic property and endothelialization, Acta Biomater. 10 (2014) 2739–2749. 10.1016/j.actbio.2014.02.042. [PubMed: 24602806]

[12]. Pedersen G, Laxdal E, Ellensen V, Jonung T, Mattsson E, Improved patency and reduced intimal hyperplasia in PTFE grafts with luminal immobilized heparin compared with standard PTFE grafts at six months in a sheep model, J. Cardiovasc. Surg. (Torino). 51 (2010) 443–448.

[13]. Abumaree M, Al Jumah M, Pace RA, Kalionis B, Immunosuppressive properties of mesenchymal stemcells, Stem Cell Rev. 8 (2012) 375–392. 10.1007/s12015-011-9312-0.

[14]. Gao F, Chiu SM, Motan D. a. L., Zhang Z, Chen L, Ji H-L, Tse H-F, Fu Q-L, Lian Q, Mesenchymalstem cells and immunomodulation: current status and future prospects, Cell Death Dis. 7 (2016) e2062. 10.1038/cddis.2015.327. [PubMed: 26794657]

[15]. Rothuizen TC, Damanik FFR, Lavrijsen T, Visser MJT, Hamming JF, Lalai RA, Duijs JMGJ, van Zonneveld AJ, Hoefer IE, van Blitterswijk CA, Rabelink TJ, Moroni L, Rotmans JI, Development and evaluation of in vivo tissue engineered blood vessels in a porcine model, Biomaterials. 75 (2016) 82–90. 10.1016/j.biomaterials.2015.10.023. [PubMed: 26491997]

[16]. Syedain Z, Reimer J, Lahti M, Berry J, Johnson S, Bianco R, Tranquillo RT, Tissue engineering ofacellular vascular grafts capable of somatic growth in young lambs, Nat. Commun. 7 (2016). 10.1038/ncomms12951.

[17]. Yun MH, Changes in Regenerative Capacity through Lifespan, Int. J. Mol. Sci. 16 (2015) 25392–25432. 10.3390/ijms161025392. [PubMed: 26512653]

[18]. Sugiura T, Matsumura G, Miyamoto S, Miyachi H, Breuer CK, Shinoka T, Tissue-engineered Vascular Grafts in Children With Congenital Heart Disease: Intermediate Term Follow-up, Semin. Thorac. Cardiovasc. Surg. 30 (2018) 175–179. 10.1053/j.semtcvs.2018.02.002. [PubMed: 29427773]

[19]. Matsuzaki Y, John K, Shoji T, Shinoka T, The Evolution of Tissue Engineered Vascular Graft Technologies: From Preclinical Trials to Advancing Patient Care, Appl. Sci. Basel Switz 9 (2019). 10.3390/app9071274.

[20]. Ahmed M, Hamilton G, Seifalian AM, The performance of a small-calibre graft for vascular reconstructions in a senescent sheep model, Biomaterials. 35 (2014) 9033–9040. 10.1016/j.biomaterials.2014.07.008. [PubMed: 25106769]

[21]. Piedrahita JA, Williams JK, Animal Models in Tissue Engineering. Part I, Tissue Eng. Part C Methods.23 (2017) 641–642. 10.1089/ten.TEC.2017.0402. [PubMed: 28938849]

[22]. Swartz DD, Andreadis ST, Animal Models for Vascular Tissue-Engineering, Curr. Opin. Biotechnol. 24 (2013) 916–925. 10.1016/j.copbio.2013.05.005. [PubMed: 23769861]

[23]. Nagiah N, Johnson R, Anderson R, Elliott W, Tan W, Highly Compliant Vascular Grafts with Gelatin-Sheathed Coaxially Structured Nanofibers, Langmuir. 31 (2015) 12993–13002. 10.1021/acs.langmuir.5b03177. [PubMed: 26529143]

[24]. Madhavan K, Elliott WH, Bonani W, Monnet E, Tan W, Mechanical and biocompatible characterizations of a readily available multilayer vascular graft, J. Biomed. Mater. Res. B Appl. Biomater. 101 (2013) 506–519. 10.1002/jbm.b.32851. [PubMed: 23165922]

[25]. Rafuse M, Xu X, Stenmark K, Neu CP, Yin X, Tan W, Layer-specific arterial micromechanics and microstructure: Influences of age, anatomical location, and processing technique, J. Biomech. 88 (2019) 113–121. 10.1016/j.jbiomech.2019.03.026. [PubMed: 31010593]

[26]. Lin J, Redies C, Histological evidence: housekeeping genes beta-actin and GAPDH are of limited value for normalization of gene expression, Dev. Genes Evol. 222 (2012) 369–376. 10.1007/s00427-012-0420-x. [PubMed: 23099774]

[27]. Nazari F, Parham A, Maleki AF, GAPDH, β-actin and β2-microglobulin, as three common reference genes, are not reliable for gene expression studies in equine adipose- and marrow-derived mesenchymal stem cells, J. Anim. Sci. Technol. 57 (2015) 18. 10.1186/s40781-015-0050-8. [PubMed: 26290738]

[28]. Glare EM, Divjak M, Bailey MJ, Walters EH, β-Actin and GAPDH housekeeping gene expression in asthmatic airways is variable and not suitable for normalising mRNA levels, Thorax. 57 (2002) 765–770. 10.1136/thorax.57.9.765. [PubMed: 12200519]

[29]. Khan SA, Tyagi M, Sharma AK, Barreto SG, Sirohi B, Ramadwar M, Shrikhande SV, Gupta S, Cell-type specificity of β-actin expression and its clinicopathological correlation in gastric

adenocarcinoma, World J. Gastroenterol. WJG. 20 (2014) 12202–12211. 10.3748/wjg.v20.i34.12202. [PubMed: 25232253]

[30]. Koobatian MT, Row S, Smith RJ Jr, Koenigsknecht C, Andreadis ST, Swartz DD, Successful endothelialization and remodeling of a cell-free small-diameter arterial graft in a large animal model, Biomaterials. 76 (2016) 344–358. 10.1016/j.biomaterials.2015.10.020. [PubMed: 26561932]

[31]. Zheng W, Wang Z, Song L, Zhao Q, Zhang J, Li D, Wang S, Han J, Zheng X-L, Yang Z, Kong D, Endothelialization and patency of RGD-functionalized vascular grafts in a rabbit carotid artery model, Biomaterials. 33 (2012) 2880–2891. 10.1016/j.biomaterials.2011.12.047. [PubMed: 22244694]

[32]. Krawiec JT, Liao H-T, Kwan L. (Lily), D'Amore A, Weinbaum JS, Rubin JP, Wagner WR, Vorp DA, Evaluation of the stromal vascular fraction of adipose tissue as the basis for a stem cell-based tissue-engineered vascular graft, J. Vasc. Surg. 66 (2017) 883–890.e1. 10.1016/j.jvs.2016.09.034. [PubMed: 28017585]

[33]. Beamish JA, Geyer LC, Haq-Siddiqi NA, Kottke-Marchant K, Marchant RE, The Effects of Heparin Releasing Hydrogels on Vascular Smooth Muscle Cell Phenotype, Biomaterials. 30 (2009) 6286–6294. 10.1016/j.biomaterials.2009.08.004. [PubMed: 19709740]

[34]. Hashimoto T, Kihara M, Sato K, Imai N, Tanaka Y, Sakai M, Tamura K, Hirawa N, Toya Y, Kitamura H, Umemura S, Heparin recovers AT1 receptor and its intracellular signal transduction in cultured vascular smooth muscle cells, FEBS Lett. 579 (2005) 281–284. 10.1016/j.febslet.2004.11.093. [PubMed: 15620727]

[35]. Stegemann JP, Nerem RM, Altered response of vascular smooth muscle cells to exogenous biochemical stimulation in two- and three-dimensional culture, Exp. Cell Res. 283 (2003) 146–155. 10.1016/s0014-4827(02)00041-1. [PubMed: 12581735]

[36]. Davies MG, Anaya-Ayala JE, El-Sayed HF, Equivalent outcomes with standard and heparin-bonded expanded polytetrafluoroethylene grafts used as conduits for hemodialysis access, J. Vasc. Surg. 64 (2016) 715–718. 10.1016/j.jvs.2016.03.443. [PubMed: 27183857]

[37]. Kim D, Chung JJ, Jung Y, Kim SH, The effect of Substance P/Heparin conjugated PLCL polymer coating of bioinert ePTFE vascular grafts on the recruitment of both ECs and SMCs for accelerated regeneration, Sci. Rep. 9 (2019) 17083. 10.1038/s41598-019-53514-6. [PubMed: 31745143]

[38]. Lynch K, Pei M, Age associated communication between cells and matrix: a potential impact on stem cell-based tissue regeneration strategies, Organogenesis. 10 (2014) 289–298. 10.4161/15476278.2014.970089. [PubMed: 25482504]

[39]. Murphy MB, Moncivais K, Caplan AI, Mesenchymal stem cells: environmentally responsive therapeutics for regenerative medicine, Exp. Mol. Med. 45 (2013) e54. 10.1038/emm.2013.94. [PubMed: 24232253]

[40]. Fukunishi T, Best CA, Ong CS, Groehl T, Reinhardt J, Yi T, Miyachi H, Zhang H, Shinoka T, Breuer CK, Johnson J, Hibino N, Role of Bone Marrow Mononuclear Cell Seeding for Nanofiber Vascular Grafts, Tissue Eng. Part A. 24 (2017) 135–144. 10.1089/ten.tea.2017.0044. [PubMed: 28486019]

[41]. Hashi CK, Zhu Y, Yang G-Y, Young WL, Hsiao BS, Wang K, Chu B, Li S, Antithrombogenic property of bone marrow mesenchymal stem cells in nanofibrous vascular grafts, Proc. Natl. Acad. Sci. 104 (2007) 11915–11920. 10.1073/pnas.0704581104. [PubMed: 17615237]

[42]. Madhavan K, Elliot W, Tan Y, Monnet E, Tan W, Performance of marrow stromal cell-seeded small-caliber multilayered vascular graft in a senescent sheep model, Biomed. Mater. 13 (2018) 055004. 10.1088/1748-605X/aac7a6. [PubMed: 29794344]

[43]. Schimke MM, Marozin S, Lepperdinger G, Patient-Specific Age: The Other Side of the Coin in Advanced Mesenchymal Stem Cell Therapy, Front. Physiol. 6 (2015) 362. 10.3389/fphys.2015.00362. [PubMed: 26696897]

[44]. Zhang J, Huang X, Wang H, Liu X, Zhang T, Wang Y, Hu D, The challenges and promises of allogeneic mesenchymal stem cells for use as a cell-based therapy, Stem Cell Res. Ther 6 (2015). 10.1186/s13287-015-0240-9.

[45]. Krawiec JT, Weinbaum JS, Liao H-T, Ramaswamy AK, Pezzone DJ, Josowitz AD, D'Amore A, Rubin JP, Wagner WR, Vorp DA, In Vivo Functional Evaluation of Tissue-Engineered Vascular Grafts Fabricated Using Human Adipose-Derived Stem Cells from High Cardiovascular Risk Populations, Tissue Eng. Part A. 22 (2016) 765–775. 10.1089/ten.tea.2015.0379. [PubMed: 27079751]

[46]. Wei Y, Wu Y, Zhao R, Zhang K, Midgley AC, Kong D, Li Z, Zhao Q, MSC-derived sEVs enhance patency and inhibit calcification of synthetic vascular grafts by immunomodulation in a rat model of hyperlipidemia, Biomaterials. 204 (2019) 13–24. 10.1016/j.biomaterials.2019.01.049. [PubMed: 30875515]

[47]. Elliott MB, Ginn B, Fukunishi T, Bedja D, Suresh A, Chen T, Inoue T, Dietz HC, Santhanam L, Mao H-Q, Hibino N, Gerecht S, Regenerative and durable small-diameter graft as an arterial conduit, Proc. Natl. Acad. Sci. 116 (2019) 12710–12719. 10.1073/pnas.1905966116. [PubMed: 31182572]

[48]. Hibino N, Duncan DR, Nalbandian A, Yi T, Qyang Y, Shinoka T, Breuer CK, Evaluation of the use of an induced puripotent stem cell sheet for the construction of tissue-engineered vascular grafts, J. Thorac. Cardiovasc. Surg. 143 (2012) 696–703. 10.1016/j.jtcvs.2011.06.046. [PubMed: 22244569]

[49]. Ding Y, Johnson R, Sharma S, Ding X, Bryant SJ, Tan W, Tethering transforming growth factor β1 to soft hydrogels guides vascular smooth muscle commitment from human mesenchymal stem cells, Acta Biomater. 105 (2020) 68–77. 10.1016/j.actbio.2020.01.034. [PubMed: 31982589]

[50]. Wingate K, Floren M, Tan Y, Tseng PON, Tan W, Synergism of matrix stiffness and vascular endothelial growth factor on mesenchymal stem cells for vascular endothelial regeneration, Tissue Eng. Part A. 20 (2014) 2503–2512. 10.1089/ten.TEA.2013.0249. [PubMed: 24702044]

[51]. Galipeau J, Sensébé L, Mesenchymal Stromal Cells: Clinical Challenges and Therapeutic Opportunities,Cell Stem Cell. 22 (2018) 824–833. 10.1016/j.stem.2018.05.004. [PubMed: 29859173]

[52]. Fitzsimmons REB, Mazurek MS, Soos A, Simmons CA, Mesenchymal Stromal/Stem Cells in Regenerative Medicine and Tissue Engineering, Stem Cells Int. 2018 (2018) 8031718. 10.1155/2018/8031718. [PubMed: 30210552]

Statement of Significance

The vascular graft is a mainstream of surgical intervention to treat vascular diseases. Currently, vascular grafts, particularly small-diameter ones, still show high failure rates. This study has evaluated the respective impacts of heparin release pattern, allogeneic bone marrow-derived stromal cell seeding, and recipient age on the long-term remodeling of vascular grafts. There is a dearth of literature which considers the recipient age as an influencing factor for vascular grafting. However, adults particularly elderly constitute the majority of vascular graft recipients in the “real” clinical environment. While juvenile animals were widely used for graft evaluations, this study involved adult animals. The study outcomes provided important implications regarding graft designs and evaluation approaches.

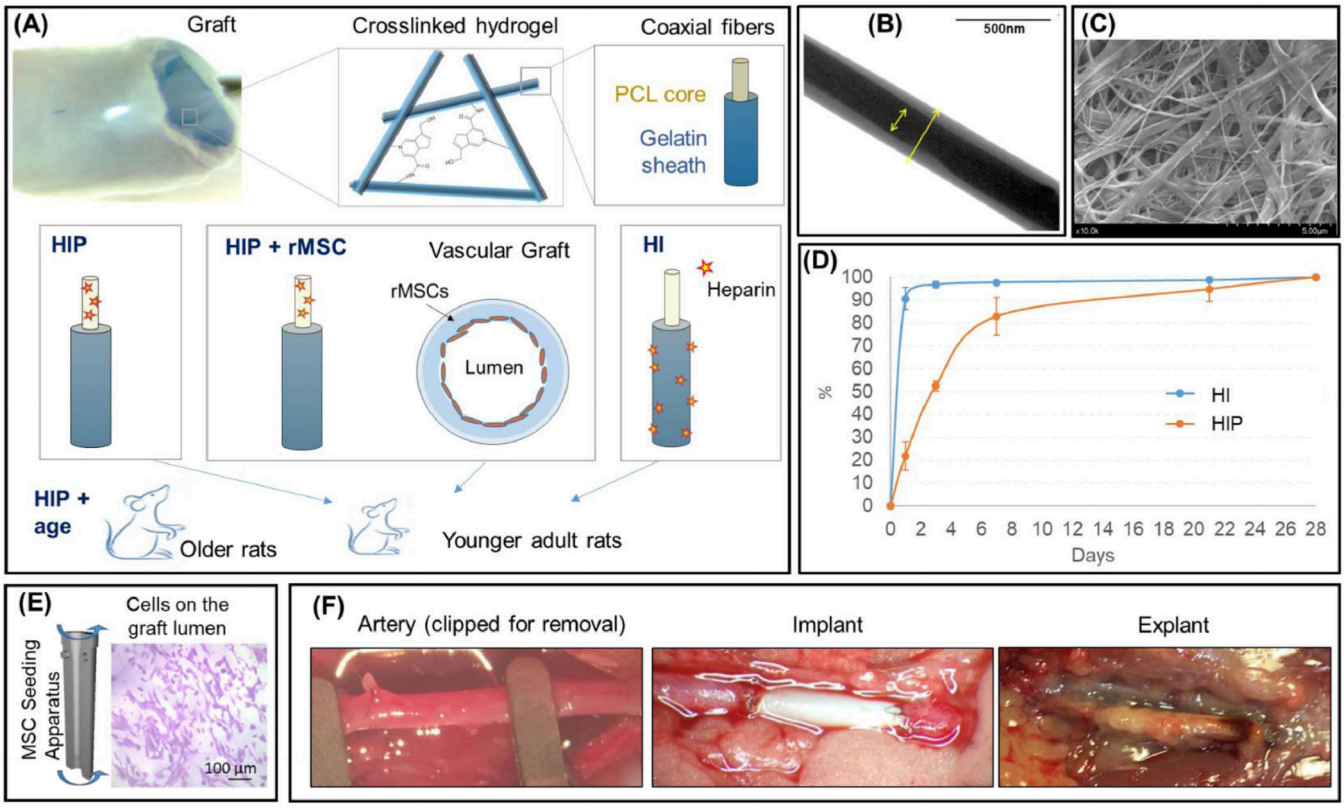

Figure 1.

Design, characterization and implantation of vascular grafts. (A) Illustration of arterial graft design (the top panel) and experimental group design (the bottom panel). Graft materials form into a genipin-crosslinked hydrogel network of coaxially-structured fibers made from poly-ε-caprolactone (PCL) and gelatin. Four experimental groups (HI, HIP, HIP+age, and HIP+ MSC) are included in the study. (B) TEM image showing the coaxial nanostructure of PCL/gelatin fibers, where PCL core appears in darker shade and gelatin sheath in lighter shade. (C) Representative SEM image of the crosslinked coaxial fiber scaffolds. (D) The cumulative heparin release profiles of HI and HIP grafts. Data at each time point shows average ± SD (n=4). (E) Illustration of the centrifugal seeding of MSCs onto the graft lumen, which are visible with crystal violet stain. (F) Representative pictures showing the implantation and explanation of interpositional artery grafts in a rat abdominal aorta model. Left: native artery was clamped and ready for sutured in place as an implant; Middle: implant sutured; Right: graft implant upon retrieval and explantation.

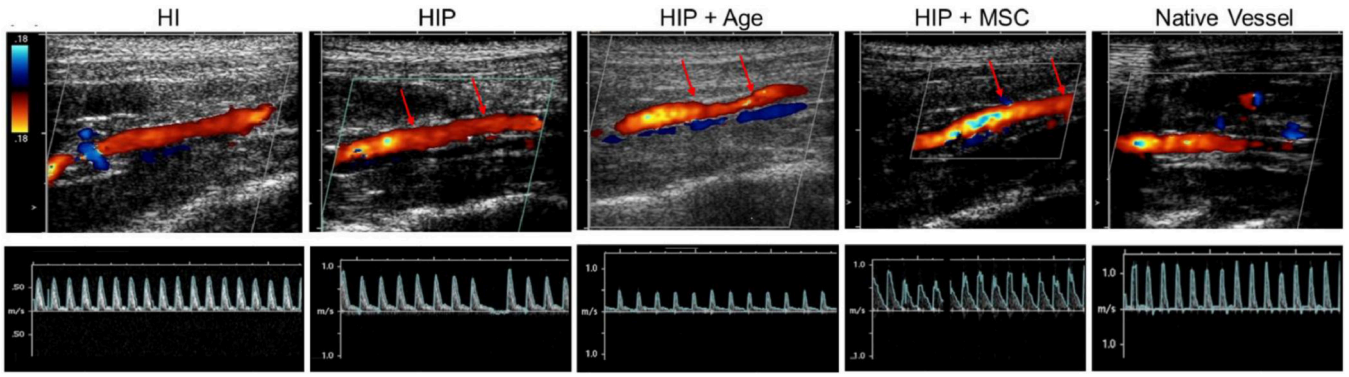

Figure 2.

Ultrasonic imaging of the blood flow perfusion in the grafts. Representative doppler ultrasound images (Top) and pulsatile flow velocity profiles (Bottom) showing the blood flow through the transverse section of the four different vascular grafts and native artery. Red arrows on the top images illustrate anastomosis sites. Direction and velocity of blood flow can be estimated from color scale on the left.

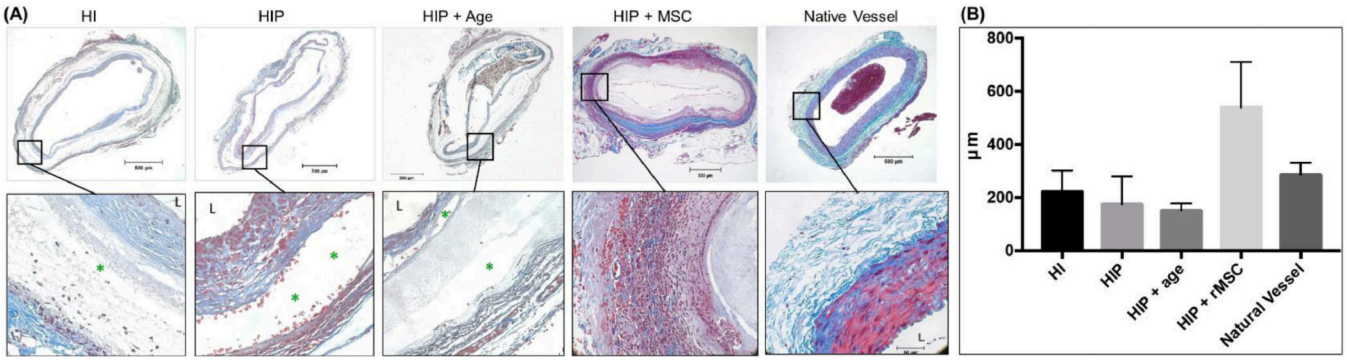

Figure 3.

Histochemical analysis of explanted grafts, showing tissue formation on the graft wall. (A) Representative images at two different magnifications showing the cross-sections of graft tissues stained with trichrome stain, which keratin and muscle fiber are in red, collagen in blue and cytoplasm in pink. In all images, the lumen is marked with “L”, while “*” shows the fracture points in the synthetic graft due to histological sectioning, a result from the difference in tissue and graft mechanics. The scale bar in top images is 500μm, and 50μm in bottom ones, (B) Tissue thickness on the graft or vessel wall, estimated from the histological images.

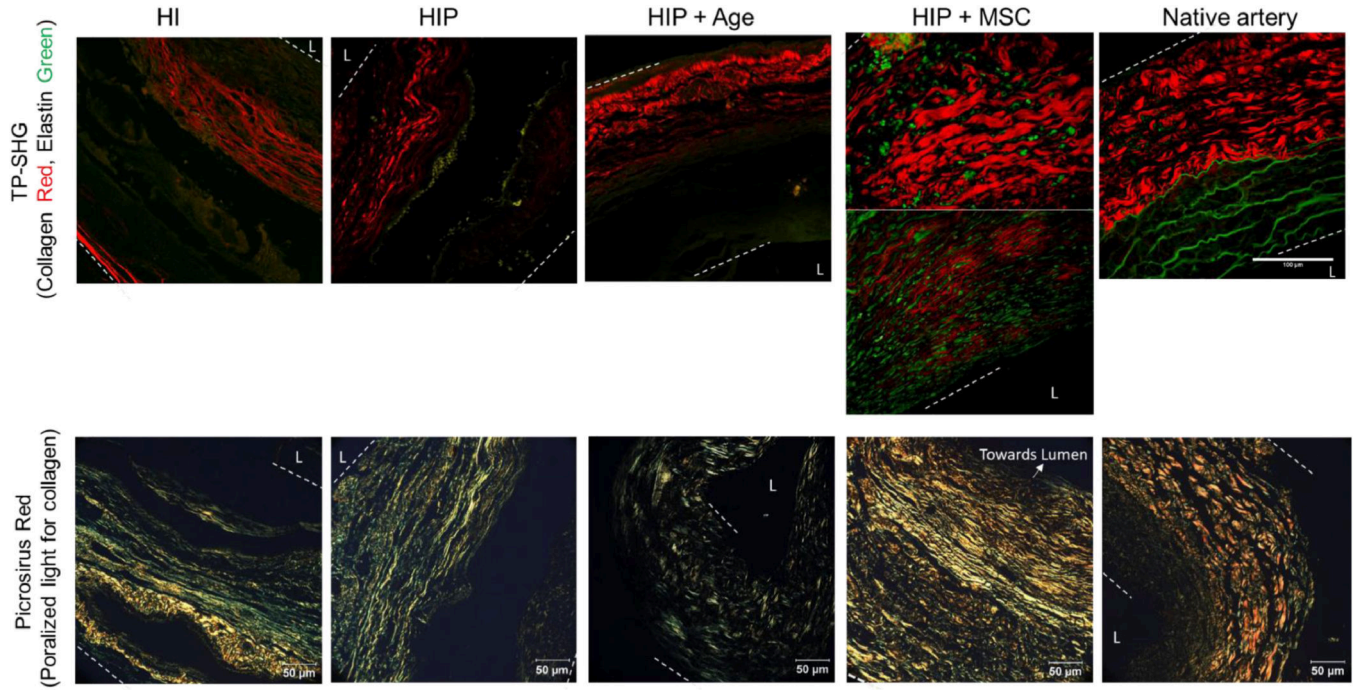

Figure 4.

Extracellular matrix remodeling on the graft wall. The top panel shows multiphoton images using combined SHG and TPEF modalities to illuminate the structure and density of collagen (red from SHG) and elastin (green from TPEF). Because the graft wall of HIP +MSC sample was much thicker, two TP-SHG images were pieced together to show both collagen and elastin fiber structure. The bottom panel shows histological images of collagen with PicroSirius red stain. All images were taken under a 40X objective. Scale bar: 50 microns. The lumen location is marked with “L”. White dashed lines showed the graft borders.

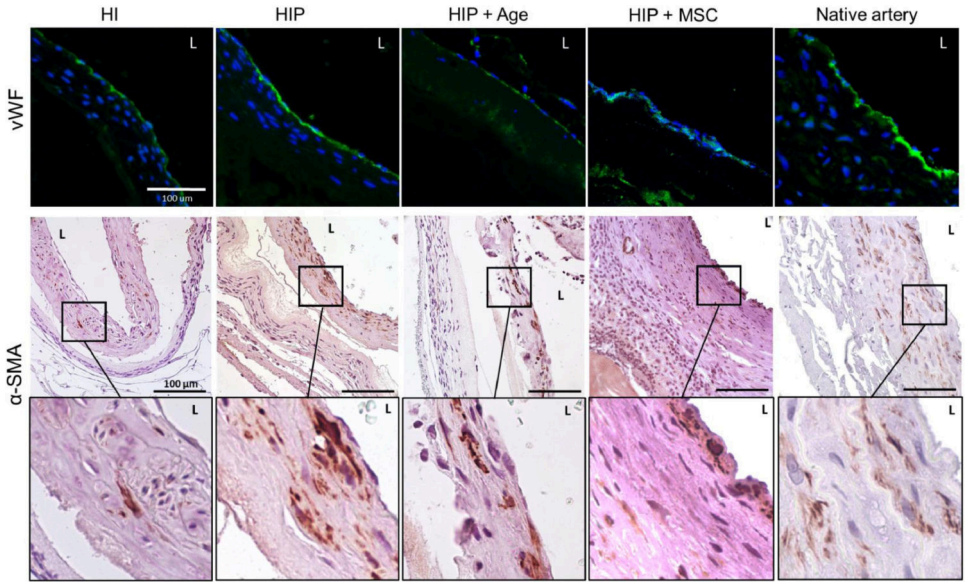

Figure 5.

Cell remodeling on the graft wall. Top panel: Immunofluorescence images of endothelial cell marker (vWF in green) and nucleus (blue). Middle and bottom panels: Immunohistochemistry images of smooth muscle cell marker (α-SMA in red) and nucleus (blue), with two different magnifications. Scale bar: 100μm

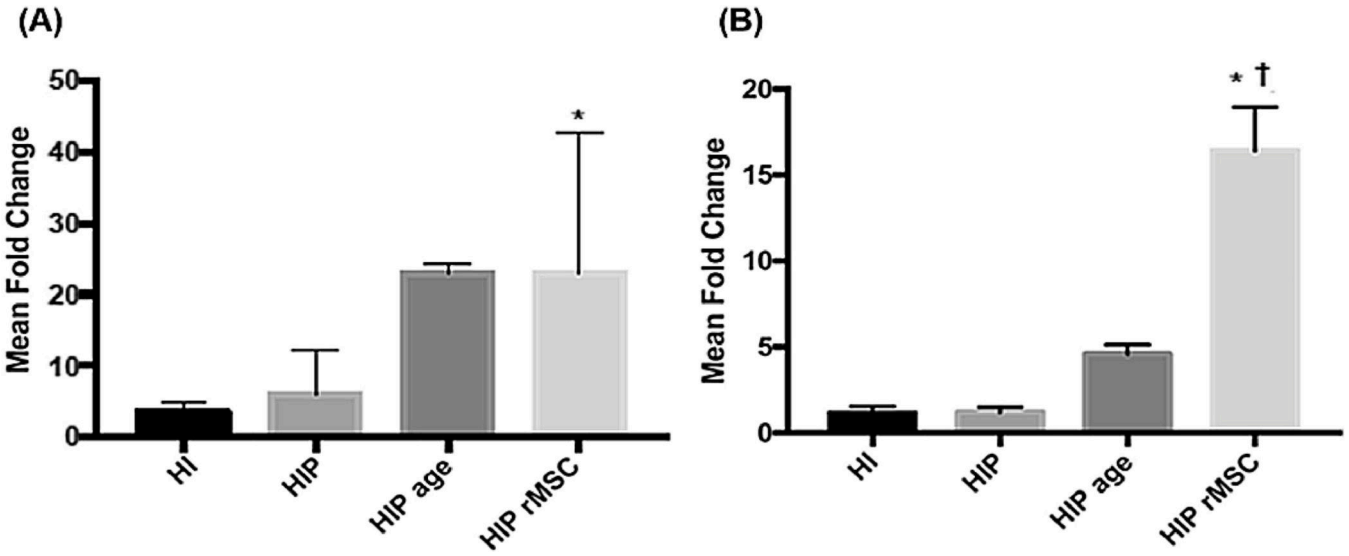

Figure 6.

Gene expression results of α-SMA (A) and elastin (B). The quantitative PCR results are from the mRNA samples extracted from the tissues on the graft wall, and the gene expression is normalized by the vWF expression due to its stable expression. '*': $p < 0.05$ compared to HI; '†': $p < 0.05$ compared to HIP.